



## Mode decomposition for multicore fibers based on far-field intensity measurements

KUNHAO JI\*

Optoelectronics Research Centre, University of Southampton, Southampton SO17 1BJ, UK  
\*K.Ji@soton.ac.uk

Received 28 November 2024; revised 7 January 2025; accepted 22 January 2025; posted 22 January 2025; published 31 January 2025

We present a mode decomposition method for multicore fibers (MCFs) that is based on intensity measurements in the far-field. Mode decomposition of several homemade multicore fibers is demonstrated in the far-field with low residual errors. Accurate measurement of supermode compositions and of the electric fields among cores is crucial for many applications involving multicore fibers as well as their integration into multimode platforms.

Published by Optica Publishing Group under the terms of the [Creative Commons Attribution 4.0 License](#). Further distribution of this work must maintain attribution to the author(s) and the published article's title, journal citation, and DOI.

<https://doi.org/10.1364/OL.550270>

Multicore fibers (MCFs) have attracted renewed interest in recent years not only to boost the transmission capacity in optical communications [1] but also due to their high performance in multi-channel propagation. Offering several degrees of freedom through diverse fiber designs, MCFs provide integration with other types of fibers and/or waveguides. At present, they have been widely employed in various applications, including long- and short-distance communications [2], optical sensing [3], image transmission and optical imaging [4], MCF amplifiers and lasers [5,6], as well as nonlinear processes such as pulse compression [7] and beam condensation [8].

MCFs support the propagation of a number of supermodes (SMs), which is proportional to the number of cores [9]. As with multimode fibers, light propagation in MCFs also suffers from modal instabilities that could result from bending [10], high transmission power [8], and nonlinear effects [11]. Because the selective excitation of supermodes is highly demanded in many applications [12], it is important to characterize the mode composition at the output of MCFs, which can provide quantitative insights into light propagation among the supermodes and across the cores. Consequently, mode decomposition (MD) of MCFs also serves as a diagnostic tool for MCF coupling in beam delivery systems.

MD is a fundamental tool in multimode optics, which provides the relative power and phase (modal coefficients) of each guided mode propagating through the fiber. Several techniques for MD have been investigated in few-mode fibers, including complex amplitude measurements [13], spectrum sweep [14], holography [15], spatial light modulator [16,17], and numerical methods

[18–22]. The latter techniques are based on intensity measurements, where the modal coefficients are estimated by comparing the reconstructed intensity distribution with the measured intensity profiles. Optimization algorithms have been successfully employed in MD of few-mode fibers [19]. Additionally, deep learning has been demonstrated in real-time MD for multimode fibers [20]. Recently, a matrix formalism method [21] has been proposed for fast MD in few-mode fibers, which is based on a transformation matrix connecting the measured output intensity distribution to the distribution of guided modes.

These MD techniques could be potentially used for mode analysis of MCFs. For example, a computer-generated hologram method has been demonstrated to analyze the output from a 19-core fiber [23]. However, this method has the limitation of high cost and low flexibility [15]. Recently, an off-axis holography method has been used for the estimation of mode content for a six-core fiber [12], but this requires a reference beam, and a detailed quantitative modal characterization remains to be investigated. These methods implement mode decomposition in the near-field (NF). However, when there are fabrication defects (non-uniform core diameters or inconsistent core spacing) or when the fiber is coiled with a small radius, the NF supermode distributions will deviate from the ideal case [24], thus limiting the MD accuracy of MCFs.

In this Letter, to the best of our knowledge, mode decomposition in multicore fibers is investigated for the first time using a numerical method based on far-field (FF) intensity measurements. Accurate MD of MCF can be achieved through a modified transformation matrix algorithm using noiseless FF intensity. An optimization algorithm (stochastic parallel gradient descent, SPGD) is employed to optimize the estimation of modal coefficients and maintain accuracy even if in the presence of intensity noises.

In order to carry on this investigation, we designed and fabricated several multicore fibers using a stack-and-draw technique, including a dual-core fiber (DCF), a triple-core fiber (TCF), a four-core fiber (4CF), and a seven-core fiber (7CF). Supermodes in these MCFs can be calculated through finite element method simulations (Comsol Multiphysics 6.0 is used). Figure 1 presents cross sections of the homemade multicore fibers and the corresponding NF and FF intensity distributions of each supermode. In these fibers, each core has a diameter of  $\sim 5 \mu\text{m}$  and the adjacent cores have a center-to-center distance of  $\sim 10 \mu\text{m}$ . Each individual core has a numerical aperture of 0.15 and only supports the propagation of the  $\text{LP}_{01}$  mode at a wavelength of

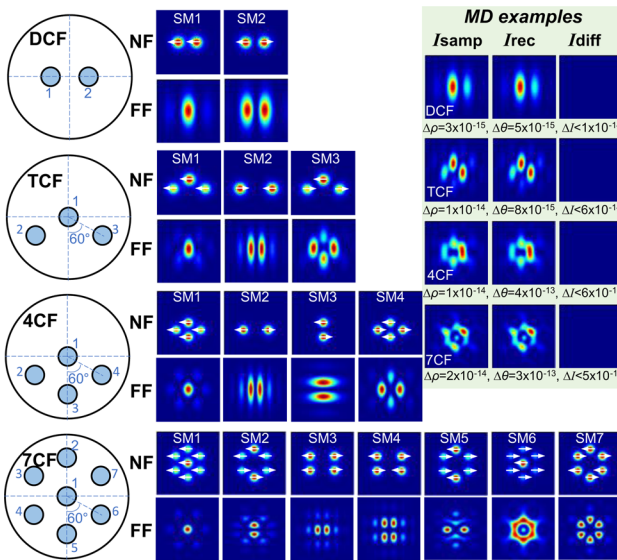


**Fig. 1.** MCF cross sections, corresponding supermode intensity distributions, and MD examples.  $I_{\text{samp}}$ : sampled intensity (normalized to maximum value);  $I_{\text{rec}}$ : reconstructed intensity (normalized to maximum value) based on MD results;  $I_{\text{diff}}$  ( $\Delta I$ ): difference between them.  $\Delta\rho$ : power error (total power normalized to 1),  $\Delta\theta$ : phase error (unit, rad).

1040 nm. In the NF, the fundamental supermode is the in-phase combination of all cores, and the highest-order supermode has adjacent cores that are in anti-phase. The FF distribution of supermodes can be obtained through the diffraction theory or the angular spectrum propagation method [25]. Note that in an MCF, different mode combinations can result in similar NF intensity distribution, such as the even (SM1) and odd (SM2) modes in the DCF, or the SM1 and SM3 modes in the TCF (see Fig. 1). This similarity can lead to significant errors in NF intensity-based mode decomposition measurements.

The output intensity distribution from an MCF is a linear combination of supermodes. The 2D output intensity profile measured by a camera (consisting of  $M \times M$  pixels) can be written as an  $M^2 \times 1$  vector with its entry [21] as follows:

$$\mathbf{I}^{(m)} = \sum_{k=1}^N \sum_{j=1}^N C_k C_j^* E_k^{(m)} E_j^{*(m)}, \quad m = 1, 2, \dots, M^2, \quad (1)$$

where  $C_{k(j)} = \sqrt{\rho_k} \exp(i\theta_k)$  is the complex modal coefficient for the  $k(j)$ th mode,  $N$  is the number of modes, and  $m$  is the pixel index. The complex amplitude of the  $k(j)$ th supermode is also written in the form of an  $M^2 \times 1$  vector, and  $E_{k(j)}^{(m)}$  is the value at the  $m$ th pixel. By defining an  $M^2 \times N^2$  transformation matrix,  $\mathbf{T}$ , that contains only the  $E_{k(j)}^{(m)}$  terms and an  $N^2 \times 1$  vector  $\mathbf{V}$  that consists of the  $C_{k(j)}$  terms, the intensity  $I$  can be written in matrix form as follows:

$$\mathbf{I} = \mathbf{T}\mathbf{V}, \quad (2)$$

$$T = \begin{bmatrix} E_1^{(1)} E_1^{*(1)} \dots E_N^{(1)} E_N^{*(1)} & E_2^{(1)} E_1^{*(1)} \dots E_N^{(1)} E_N^{*(1)} & \dots & E_N^{(1)} E_1^{*(1)} \dots E_N^{(1)} E_N^{*(1)} \\ \vdots & \vdots & & \vdots \\ E_1^{(m)} E_1^{*(m)} \dots E_1^{(m)} E_N^{*(m)} & E_2^{(m)} E_1^{*(m)} \dots E_2^{(m)} E_N^{*(m)} & \dots & E_N^{(m)} E_1^{*(m)} \dots E_N^{(m)} E_N^{*(m)} \\ \vdots & \vdots & & \vdots \\ E_1^{(M^2)} E_1^{*(M^2)} \dots E_1^{(M^2)} E_N^{*(M^2)} & E_2^{(M^2)} E_1^{*(M^2)} \dots E_2^{(M^2)} E_N^{*(M^2)} & \dots & E_N^{(M^2)} E_1^{*(M^2)} \dots E_N^{(M^2)} E_N^{*(M^2)} \end{bmatrix} \quad (3)$$

$$\mathbf{V} = [C_1 C_1^* \dots C_1 C_N^* \quad C_2 C_1^* \dots C_2 C_N^* \quad \dots \quad C_N C_1^* \dots C_N C_N^*]^T. \quad (4)$$

The vector  $\mathbf{V}$  is therefore computed as  $\mathbf{V} = \mathbf{T}^{-1} \mathbf{I}$ , with  $\mathbf{T}^{-1}$  as the pseudoinverse matrix of  $\mathbf{T}$ . The relative power ( $\rho_k$ ) and relative phase ( $\theta_k$ ) of the  $k$ th mode can be determined from Eq. (4), assuming  $\theta_1 = 0$  [21], as follows:

$$\rho_k = \frac{\mathbf{V}[N(k-1)+k]}{\sum_{k=1}^N \mathbf{V}[N(k-1)+k]}, \quad k = 1, 2, \dots, N, \quad (5)$$

$$\theta_k = \text{acos} \left( \frac{\mathbf{V}[k] + \mathbf{V}[N(k-1)+1]}{2\sqrt{\rho_1 \rho_k}} \right), \quad k = 2, \dots, N. \quad (6)$$

Equations (5) and (6) yield error-negligible MD results for MCFs in the far-field, as demonstrated by the simulation examples shown in Fig. 1, where the sampled electric field is generated by the combination of supermodes with random relative powers and phases. The negligible MD errors ( $\Delta\rho$ ,  $\Delta\theta$ ) and low discrepancy ( $\Delta I$ ) between the reconstructed ( $I_{\text{rec}}$ ) and sampled ( $I_{\text{samp}}$ ) intensities indicates the accuracy of this method.  $I_{\text{samp}}$  ( $I_{\text{rec}}$ ) is obtained by substituting the sampled (calculated) modal coefficients into Eq. (1), respectively. The MD errors are defined as the weighted average over all the guided modes:

$$\Delta\rho = \sum_{k=1}^N (|\rho_{\text{calc},k} - \rho_{\text{samp},k}| \rho_{\text{samp},k}), \quad (7)$$

$$\Delta\theta = \sum_{k=1}^N \left( |\theta_{\text{calc},k} - \theta_{\text{samp},k}| \frac{|\theta_{\text{samp},k}|}{\sum_{k=1}^N |\theta_{\text{samp},k}|} \right), \quad (8)$$

where  $\rho_{\text{calc(samp),k}}$  and  $\theta_{\text{calc(samp),k}}$  represents the calculated (sampled) relative mode power and phase for the  $k$ th mode, respectively. It is worth pointing out that in Ref. [21], a similar transformation matrix method was investigated for few-mode fibers in the near-field. However, the approximation  $E_k^{(m)} E_j^{*(m)} \sim E_j^{(m)} E_k^{*(m)}$  utilized in Ref. [21] is not valid for the FF supermodes in MCFs.

In practical applications, we need to investigate the robustness of the MD algorithm against the quality of the measured intensity profile (which is influenced by noise, aberration, spectral-linewidth, and camera resolution), as well as the definition of supermode distributions (deviation due to fabrication imperfections) and the choice of the image center.

Figure 2 displays the MD error analysis for the homemade MCFs under test. Each dot represents the averaged MD errors of 200 simulations with the sampled intensity generated by superposing all supermodes with random relative powers and phases. Uniformly distributed random intensity noise is added to the sampled intensity, characterized by a signal-to-noise ratio (SNR) of 10–40 dB.

Four MD algorithms are compared: *Matrix-ref* is the method introduced in Ref. [21]; *Matrix-new* is the method introduced in this manuscript, as described in Eqs. (1)–(6); *SPGD* is an optimization method introduced in Ref. [19], where the modal coefficients can be obtained from random initial values; and *Matrix-new + SPGD* is the optimization based on the *Matrix-new* with the support of *SPGD*.

Figure 2 shows that both averaged power and phase errors can be suppressed across different SNRs and across different number of cores by using the *Matrix-new + SPGD* method (see green dots), which generally outperforms the other algorithms. The mode power error is less than 2% and the relative phase error can be suppressed below 0.3 rad for the fibers under test

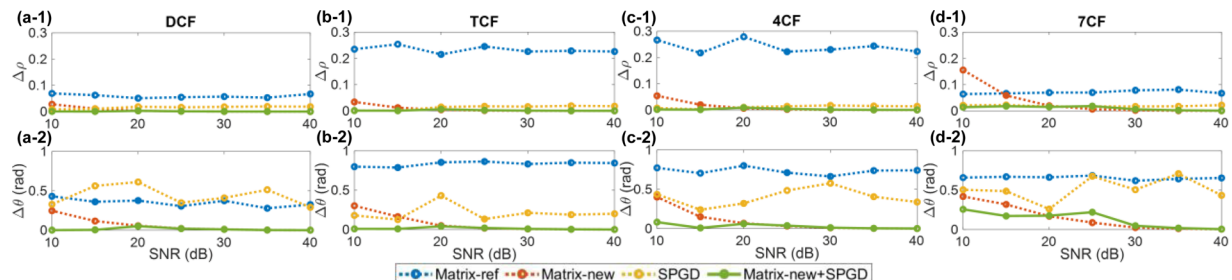


**Fig. 2.** Mode decomposition error analysis for the MCFs under test at different noise levels. (a-1)–(d-1) Averaged mode power errors of 200 simulations. (a-2)–(d-2) Averaged mode phase errors of 200 simulations. The image size is  $1400 \times 1400$  pixels in the simulations, with a pixel size of  $5.5 \mu\text{m}$ .

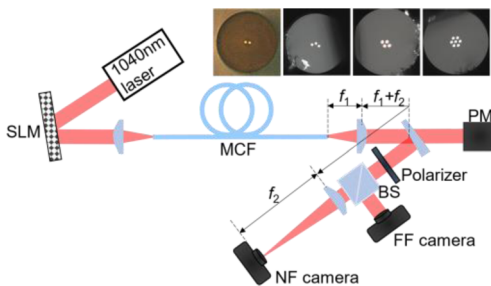


**Fig. 3.** Experimental setup and cross-section images of MCFs under test. An SLM is used for coupling into the MCF. The MCF output is sampled by a wedge prism and then imaged on FF and NF cameras. A linear polarizer is used to select one polarization. BS: beam splitter.

with  $\text{SNR} > 10 \text{ dB}$ . A higher SNR of the measured intensity profile could further compensate MD errors, especially for the fibers with more cores. When the SNR is larger than  $20 \text{ dB}$ , the *Matrix-new* method can already provide high-precision mode decomposition for up to seven-core fibers. In addition, the *Matrix-new* method provides appropriate initial values for SPGD optimization, with the further benefits of shorter convergence time and less local optimum (see the comparison between *SPGD* and *Matrix-new + SPGD* in Fig. 2).

To verify our mode decomposition method, an experimental setup was implemented to collect the output intensity profiles from the DCF, TCF, 4CF, and 7CF, as shown in Fig. 3. A linearly polarized  $0.5 \text{ ns}$ -pulsed fiber laser, operating at a repetition rate of  $800 \text{ kHz}$ , is coupled into the test fiber via a spatial light modulator (SLM). By properly setting the phase pattern displayed on the SLM screen, light can be coupled into different fiber cores with specific powers and phases to selectively excite random combinations of supermodes. The fiber output power is monitored on a power meter (PM), and a portion of the output is reflected by a wedge prism for beam profile measurement. An FF camera is used to collect the FF intensity profiles used for mode decomposition. As the fiber may be rotated, the core distribution at the output facet may not be consistent with the distribution shown in Fig. 1. A NF camera placed in a 4-f system configuration (see Fig. 3) measures the NF beam profiles, which are used for identifying the rotation of fiber as well as the core-to-core distance. The focal lengths of the two lenses are  $f_1 = 13.8 \text{ mm}$  and  $f_2 = 500 \text{ mm}$ , corresponding to a magnification factor of  $\sim 36x$ . The pixel size of the cameras is  $5.5 \mu\text{m}$ , and the captured image was cropped to the size of  $1088 \times 1088$  pixels. The analog-to-digital converter level of the camera is

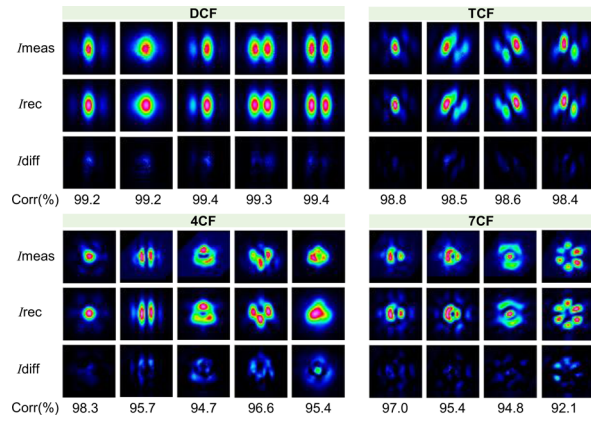


**Fig. 4.** Experimental results for MCFs under test. Each column displaying the comparisons between the measured and reconstructed intensity profiles ( $I_{\text{meas}}$  and  $I_{\text{rec}}$ , both normalized to maximum value), along with their difference ( $I_{\text{diff}}$ ), and correlation factors (Corr).

12 bits, corresponding to a total of 4096 intensity levels. After appropriate modifications (rotation and core spacing) on the NF supermode distributions, the FF supermode distributions can be obtained using the angular spectrum propagation method. Due to the short fiber lengths ( $< 1 \text{ m}$ ) used in the experiments and good birefringence produced by the non-circularly symmetric core arrangements, the MCF output beam can maintain the input linear polarization and has a high polarization extinction ratio  $> 10 \text{ dB}$ . A linear polarizer is used to select the polarization. It is worth noting that a polarization beam splitter can be employed to measure the intensity profiles of two polarizations simultaneously, so as to achieve both polarization and mode decomposition.

Figure 4 displays several experimental results for different MCFs at an average output power of  $\sim 2 \text{ W}$ . The optical SNR at the  $1040 \text{ nm}$  wavelength is higher than  $20 \text{ dB}$ , ensuring that the measured beam profiles are not affected by other spectral components. The measured FF intensity profiles and calculated FF complex amplitudes of each supermode were written in the form of  $M^2 \times 1$  vectors and then substituted into Eq. (2) to obtain the vector  $V$ , yielding the modal coefficients ( $\rho_k$  and  $\theta_k$ ). The measured images have a SNR of  $\sim 15 \text{ dB}$ , which was calculated as the standard deviation of the intensity values in the pixels outside the main beams [21]. The estimation of the modal coefficients was therefore optimized via a SPGD algorithm to further minimize the discrepancy between the measured

**Table 1. Modal Coefficients for the Measurements in Fig. 4**

Fiber	DCF					TCF			
$\rho$	0.93,	0.73,	0.62,	0.32,	0.08,	0.98,	0.18,	0.06,	0.22,
[SM1,	0.07	0.27	0.38	0.68	0.92	0.02,	0.39,	0.49,	0.57,
SM2,						0	0.43	0.45	0.21
...]									
$\theta(\text{rad})$	0,	0,	0,	0,	0,	0,	0,	0,	0,
[SM1,	1.85	1.63	0.66	1.64	1.93	1.88,	1.08,	3.74,	2.81,
SM2,						2.72	1.99	1.57	1.27
...]									
Fiber	4CF					7CF			
$\rho$	0.86,	0.02,	0.23,	0.17,	0.59,	0.04,	0,	0.47,	0.09,
[SM1,	0,	0.85,	0,	0.01,	0,	0.14,	0.34,	0.03,	0.02,
SM2,	0.08,	0,	0.55,	0.28,	0.24,	0.74,	0.58,	0.01,	0.13,
...]	0.06	0.13	0.22	0.54	0.17	0.01,	0.06,	0.06,	0.18,
						0,	0.02,	0.05,	0,
						0.07,	0, 0	0.37,	0.01,
						0	0.01	0.57	
$\theta(\text{rad})$	0,	0, 1.1,	0,	0,	0,	0, 5.2,	0,	0, 4.9,	0, 1.8,
[SM1,	0.62,	0.8,	1.17,	4.48,	0.71,	0.3,	-2.01,	1.5,	5.01,
SM2,	0.16,	2.8	0.78,	0.14,	0.45,	2.3,	5.82,	3.22,	4.99,
...]	5.75		0.64	5.82	0.27	3.02,	1.3,	0.57,	1,
						1.59,	3.68,	4.6,	5.32,
						1.74	2.9,	6.2	3.25
						4.31			

and reconstructed intensity profiles. Figure 4 shows high mode decomposition accuracy and the mean correlation factor (Corr, [18]) between the reconstructed and measured intensity profiles is 99.3%, 98.6%, 96.4%, and 94.8% for the DCF, TCF, 4CF, and 7CF, respectively. The degraded correlation in 4CF and 7CF could result from intensity noises, aberrations, and fabrication imperfections. The calculated modal coefficients of each supermode in these fibers are listed in Table 1. The relative mode powers and relative mode phases in each column correspond to the measurements in each column of Fig. 4.

Mode decomposition over supermodes also provides an effective way to estimate the phase information of the individual cores. According to the coupled mode theory, we can derive a relationship matrix,  $\mathbf{R}$ , that connects the supermode distribution to the electric field in each core [26] as follows:

$$[E_{c1} \ E_{c2} \ \cdots \ E_{cN}]^T = \mathbf{R} [\sqrt{\rho_1} e^{i\theta_1} \ \sqrt{\rho_2} e^{i\theta_2} \ \cdots \ \sqrt{\rho_N} e^{i\theta_N}]^T, \quad (9)$$

where  $E_{ck}$  is the electric field in the  $k$ th core with its phase determined by  $\arg(E_{ck})$ , and  $\mathbf{R}$  is a  $N \times N$  matrix. The matrix  $\mathbf{R}$  strictly depends on the core arrangement. For example, in the case of the 4CF under test, the matrix  $\mathbf{R}$  is given by Eq. (10), with the core indices labeled in Fig. 1. Equation (9) indicates that the electric field in the individual cores can be evaluated from our MD method.

$$\mathbf{R}_{4CF} = \frac{1}{4} \begin{bmatrix} \sqrt{5} & 0 & 2\sqrt{2} & \sqrt{3} \\ \sqrt{3} & 2\sqrt{2} & 0 & -\sqrt{5} \\ \sqrt{5} & 0 & -2\sqrt{2} & \sqrt{3} \\ \sqrt{3} & -2\sqrt{2} & 0 & -\sqrt{5} \end{bmatrix}. \quad (10)$$

In conclusion, in this Letter we proposed a mode decomposition method for multicore fibers using FF intensity measurements.

We have demonstrated mode decomposition with strong suppression of error even when dealing with noisy images. We have successfully demonstrated mode decomposition in several MCFs with the number of cores of up to  $N=7$ . The reported method can provide a quantitative characterization of not only the mode composition in MCFs but also the electric field distribution in the cores, representing a significant step forward in advancing the potential of MCFs for future photonic devices and applications.

**Funding.** H2020 European Research Council (802682).

**Acknowledgment.** K. Ji thanks Massimiliano Guasoni for support throughout the development of this research. I would also like to thank Ian Davidson for fabricating the multicore fibers.

**Disclosures.** The author declares no conflicts of interest.

**Data availability.** The data for this work is accessible through the University of Southampton Institutional Research Repository [27].

## REFERENCES

- D. J. Richardson, J. M. Fini, and L. E. Nelson, *Nat. Photonics* **7**, 354 (2013).
- B. J. Puttnam, G. Rademacher, and R. S. Luís, *Optica* **8**, 1186 (2021).
- H. Zhang, Z. Wu, P. Shum, *J. Opt.* **18**, 085705 (2016).
- N. Stasio, C. Moser, and D. Psaltis, *Opt. Lett.* **41**, 3078 (2016).
- A. Klenke, C. Jauregui, A. Steinkopff, *Prog. Quantum Electron.* **84**, 100412 (2022).
- K. Ji, D. Lin, I. A. Davidson, *Photonics Res.* **11**, 181 (2023).
- A. M. Rubenchik, I. S. Chekhovskoy, M. P. Fedoruk, *Opt. Lett.* **40**, 721 (2015).
- E. J. Bochave, P. K. Cheo, and G. G. King, *Opt. Lett.* **28**, 1200 (2003).
- I. Kaminow, T. Li, and A. E. Willner, *Optical Fiber Telecommunications Volume VIB: Systems and Networks* (Academic Press, 2013).
- S. García, M. Ureña, and I. Gasulla, *Opt. Express* **27**, 31290 (2019).
- K. Ji, I. Davidson, J. Sahu, *Nat. Commun.* **14**, 7704 (2023).
- A. V. Andrianov, N. A. Kalinin, E. A. Anashkina, *J. Lightwave Technol.* **38**, 2464 (2020).
- M. Paurisse, L. Lévèque, M. Hanna, *Opt. Express* **20**, 4074 (2012).
- J. W. Nicholson, A. D. Yablon, S. Ramachandran, *Opt. Express* **16**, 7233 (2008).
- M. Lyu, Z. Lin, G. Li, *Sci. Rep.* **7**, 6556 (2017).
- D. Flamm, D. Naidoo, C. Schulze, *Opt. Lett.* **37**, 2478 (2012).
- M. D. Gervaziev, I. Zhdanov, D. S. Kharenko, *Laser Phys. Lett.* **18**, 015101 (2021).
- R. Bruning, P. Gelszinnis, C. Schulze, *Appl. Opt.* **52**, 7769 (2013).
- L. Huang, S. Guo, J. Leng, *Opt. Express* **23**, 4620 (2015).
- Y. An, L. Huang, J. Li, *IEEE J. Sel. Top. Quant.* **26**, 1 (2020).
- E. S. Manuylovich, V. V. Dvoyrin, and S. K. Turitsyn, *Nat. Commun.* **11**, 5507 (2020).
- Y. Liu, Q. Liu, J. Xiong, *Opt. Lett.* **47**, 5813 (2022).
- C. Schulze, O. A. Schmidt, D. Flamm, *Proc. SPIE* **7914**, 79142H (2011).
- T. Sakamoto, T. Mori, M. Wada, *J. Lightwave Technol.* **34**, 1228 (2016).
- J. W. Goodman, *Introduction to Fourier Optics* (Roberts & Company publishers, 2005).
- K. Ji, D. J. Richardson, S. Wabnitz, *“Sub-nanosecond all-optically reconfigurable photonics in optical fibres,” arXiv* (2024).
- K. Ji, “Data supporting the publication ‘Mode decomposition for multicore fibers based on far-field intensity measurements’,” Univ. of Southampton (2025), <https://eprints.soton.ac.uk/497470/>.